International Journal of Solids and Structures 46 (2009) 677–697

Contents lists available at ScienceDirect

International Journal of Solids and Structures

journal homepage: www.elsevier.com/locate/ijsolstr

Finite element micromechanics model of impact compression of closed-cell polymer foams

N.J. Mills [a,*], R. Stämpfli [b], F. Marone [c], P.A. Brühwiler [b]

[a] Metallurgy and Materials, University of Birmingham, B15 2TT Edgbaston, Birmingham, UK
[b] EMPA, Swiss Federal Laboratories for Materials Testing and Research, St Gallen, Switzerland
[c] Swiss Light Source, Paul Scherrer Institut, Villigen, Switzerland

ARTICLE INFO

Article history:
Received 18 October 2007
Received in revised form 18 August 2008
Available online 22 September 2008

Keywords:
Foam structures
Impact
Mechanical properties
Modelling

ABSTRACT

Finite element analysis, of regular Kelvin foam models with all the material in uniform-thickness faces, was used to predict the compressive impact response of low-density closed-cell polyethylene and polystyrene foams. Cell air compression was analysed, treating cells as surface-based fluid cavities. For a typical 1 mm cell size and 50 s^{-1} impact strain rate, the elastic buckling of cell faces, and pop-in shape inversion of some buckled square faces, caused a non-linear stress strain response before yield. Pairs of plastic hinges formed across hexagonal faces, then yield occurred when trios of faces concertinaed. The predicted compressive yield stresses were close to experimental data, for a range of foam densities. Air compression was the hardening mechanism for engineering strains <0.6, with face-to-face contact also contributing for strains >0.7. Predictions of lateral expansion and residual strains after impact were reasonable. There were no significant changes in the predicted behavior at a compressive strain rate of 500 s^{-1}.

1. Introduction

Closed-cell low-density polymer foams are used for protective packaging of goods in transit, and in personal protective equipment (Gibson and Ashby, 1997; Mills, 2007a). Hence the mechanics of their compressive response at impact strain rates needs to be understood, and deformation mechanisms identified. A typical mean strain rate, for 50 mm thick foam impacted at 5 m s^{-1} to 70% compressive strain, is 50 s^{-1}. For consumer goods packaging that undergoes multiple impacts polyethylene or polypropylene foams are often used, because of their good recovery after impact. Polystyrene foam, in contrast, has a relatively poor recovery after impact, but has a high specific energy absorption, partly explaining its extensive use in protective helmets (Di Landro et al., 2002; Willinger et al., 2000).

Stauffer (2007) found that the compressive yield stresses of expanded polystyrene (EPS) bead foams, of densities 15, 30 and 50 kg m^{-3}, were 20% higher for an impact velocity of 9 ms^{-1}, than for a compressive test at 0.075 ms^{-1}. Hence the stress increase, for a factor of ten increase in strain rate, is relatively small. Ouellet et al. (2006) found a critical strain rate, circa 1000 s^{-1}, above which the strain rate sensitivity of the yield stress of EPS increased, but could not explain this phenomenon. Song et al. (2005) noted a similar effect above about 100 s^{-1} for the modulus of EPS of density 400 kg m^{-3}. There have been no direct observations of deformation mechanisms of cells, in the interior of samples, during impact compression of such foams. However, deformation mechanisms have been identified by scanning electron microscopy (SEM) of samples cut from foams, after impact compression – polystyrene cell faces concertina, with several 'plastic hinge' folds perpendicular to the

* Corresponding author. Tel./fax: +44 121 414 5185.
E-mail address: n.j.mills@bham.ac.uk (N.J. Mills).

0020-7683/$ - see front matter © 2008 Elsevier Ltd. All rights reserved.
doi:10.1016/j.ijsolstr.2008.09.012

impact direction. In foamed high density polyethylene (HDPE), recovery occurred for a long time after impact (Loveridge and Mills, 1991), driven by the viscoelastic response of the polymer.

In EPS foam, the volume fraction of open channels between the fused beads is usually only a few %, and finite element analysis (FEA) (Mills and Gilchrist, 2007) predicted that the compressive yield stress was only a few % lower than in homogenous foams of the same density. Almanza et al. (2001) found that Zotefoam low-density polyethylene (LDPE) foams, of densities in the range 15–70 kg m^{-3}, had volume fractions of polymer in the cell edges ranging from 0.16 to 0.35. Mills and Zhu (1999) measured a face volume fraction = 0.98 for EPS of density 20 kg m^{-3} and 0.93 for LDPE foam of density 24 kg m^{-3}. These foams are produced by the expansion of highly viscous polymer melts, the expanding faces drawing polymer out of the edge regions. Consequently, the edge widths are small compared with the cell diameter.

The modelling of closed-cell polymer foam compression is less advanced than that of open-cell foams (Mills, 2007a). Although both the air and the polymer structure contribute to the foam compressive stress, it is often assumed that the latter contribution (σ_P) is constant post-yield, while interactions between gas compression and the polymer structure are ignored. Hence, the compressive engineering stress σ can be written

$$\sigma = \sigma_P + \frac{p_0 \varepsilon}{1 - \varepsilon - R} \tag{1}$$

where p_0 is the gas pressure in the undeformed foam, ε the engineering compressive strain and R the foam relative density. These foams yield when the stress reaches a near-plateau level (the modelling shows later that this involves coordinated concertinaing of neighbouring faces after the formation of plastic hinges). The third term in Eq. (1) was first suggested by Rusch (1970) who, however, assumed that σ_P varied with strain. The term can be derived from a static analysis of isothermal gas compression, assuming the foam Poisson's ratio is zero. In most polymer foams, air diffusion over weeks of storage means that p_0 is equal to atmospheric pressure. Rusch's approach was taken further by Avalle et al. (2007) who examined how five empirical constants, used to fit stress–strain curves, varied with foam density. In contrast, micromechanics models avoid empirical constants, and reveal the contributions of foam deformation mechanisms.

Computationally-simple regular foam models, with uniform cell sizes and packing arrangements, are often preferred to irregular models, although real foams have a range of cell sizes and shapes. Mills and Zhu (1999) made a static analysis of the compression of a Kelvin closed-cell foam model in the [001] direction. This ignored dynamic interactions between cell pressures and polymer deformation. The collapse mechanism was assumed; only cell faces yielded, under tension in directions perpendicular to the applied compressive stress. The cell edges were assumed to act as Bernoulli beams, supported by faces which acted as membranes. The volume fraction of polymer in the edges needed to exceed 40% for the numerical model to converge. The deformation was assumed to be homogeneous on scales larger than the cell diameter, so a small representative unit cell (RUC) could be used for the whole foam. The predicted compressive stress–strain curves were similar to experimental data for LDPE foam, but higher by a factor of two for EPS foam. Neither face-to-face contact at high compressive strains, nor the response on unloading, was considered. Gibson and Ashby (1997) referred to the rise in stress at high compressive strains as 'densification', attributing it to face-to-face contact and the cell face material being compressed. However their treatment of the 'densification' contribution to the stress is empirical; the challenge remains to predict the stress increase using a micro-mechanics model.

Santosa and Wierzbicki (1998), using a truncated-cube closed-cell model for aluminium foams, predicted compressive collapse by the co-ordinated folding of four linked faces, after some face plasticity near the model vertices. McKown (2005) performed FEA of a Kelvin closed-cell foam model compressed in the [001] direction, at a strain rate of circa

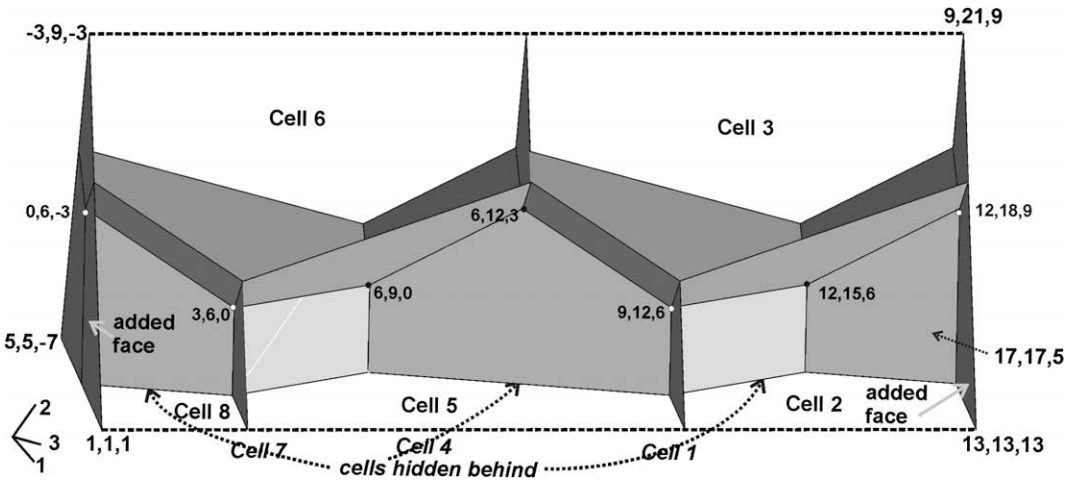

Fig. 1. Two-cell high model for [111] direction compression of a dry Kelvin foam, with vertex and prism corner coordinates in units of 1/12. Mirror symmetry planes, at the prism sides, lie between the dashed lines.

$10\ s^{-1}$, with faces simulated by shell elements. His model ignored the air pressure inside the cells, so the predicted deformation sequence (crumpling progressing from face to face, in the direction of compression) was probably unrealistic. Here his approach is extended, by considering cell gas pressures and another deformation direction.

Zheng et al. (2005) predicted that the in-plane crushing of irregular 2D aluminium honeycombs becomes more localised at higher strain rates. Deshpande and Fleck (2000) discussed whether the micro-inertia of individual cell walls caused a change in deformation mechanism with increasing strain rate, but found this not to occur in aluminium foams. Here micro-inertial effects are sought in polymer foams. Mills and Gilchrist (1997) performed finite-difference modelling of heat transfer between the cell air and the polymeric cell faces. Their predictions, when compared with the response of LDPE foams, showed that the cell air remained almost isothermal at strain rates circa $50\ s^{-1}$, due to the cell face surface area being high relative to the cell air volume, in typical foams with cell diameters less than 1 mm.

2. Finite element analysis

2.1. The choice of a finite element model

The aim is to predict the dynamic high-strain compressive response of representative polymeric closed-cell foams, including their recovery on unloading, from the foam geometry and the material properties. For the most part, a model for the [1 1 1] direction compression of a Kelvin, closed-cell, foam (Fig. 1) will be used, because the predicted response of the related open-cell model (Mills, 2007b) was close to the experimental response of polyurethane foams. Cell edges, in both that model and in compressed polyurethane foam, twisted and bent. In the static (implicit) FEA of the open-cell Kelvin model (Mills, 2007b), periodic end conditions on the prism allowed it to represent a foam of infinite extent. In contrast, the dynamic (explicit) FEA models (Figs. 1 and 2) represent infinite-layer foam samples, of thickness 2 or 4-cell diameters in the direction

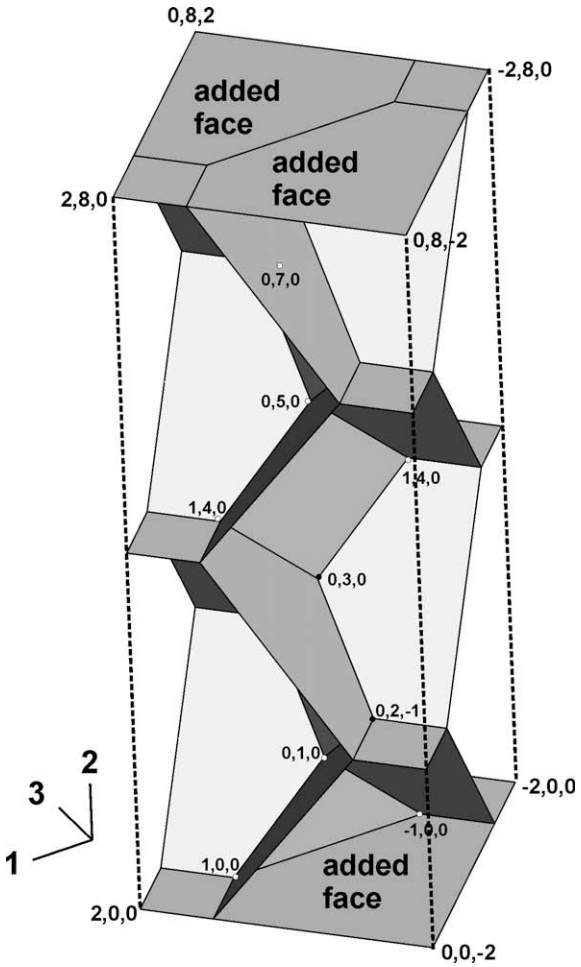

Fig. 2. Two cell high FEA model for [0 0 1] direction compression of a dry Kelvin foam with vertex and prism corner coordinates in units of 1/4. At the sides, mirror symmetry planes lie between the dashed lines.

of compression. The limited thickness reduces the number of elements and the task of defining the cell surfaces in ABAQUS CAE. However, the model must simulate the observed deformation mechanisms in the polymer foams.

FEA models can avoid the approximations of Mills and Zhu's (1999) model, and examine whether progressive cell collapse (a form of strain inhomogeneity on a cell size scale) occurs. The compressed gas in foam cells stores significant elastic energy; dynamic (explicit) FEA can model the propagation of pressure pulses through the foam during compressive impacts. The cell air was treated as isothermal, for the reasons given in the introduction.

Initially the foam Poisson's ratio was assumed to be zero, to simplify the boundary conditions in the FEA. This is a reasonable approximation post-yield, where the Poisson's ratio of compressed LDPE and EPS foams is close to zero (Mills, 2007a). However, as constraining the pre-yield deformation may change the mode of collapse, later the assumption was relaxed (and the effects shown to be minor). The model should have a similar, low, anisotropy to real foams. Therefore simulations were made in more than one direction, to assess the model anisotropy.

2.2. Geometry of Kelvin foam models

Soap foams are described as *dry* foams, when the volume fraction of water in the edges tends to zero, and as *wet* foams if the volume fraction is finite. The dry Kelvin foam consists of identical tetrakaidecahedral cells, each with eight hexagonal and six square planar faces, arranged in a body centre cubic array. The foam geometry can be constructed from vertex positions,

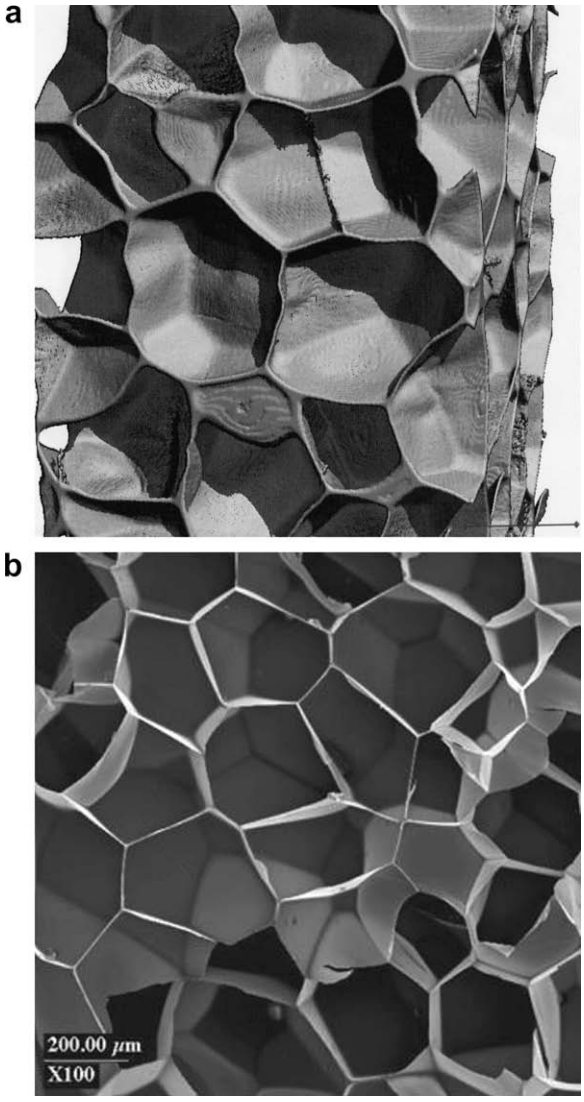

Fig. 3. (a) Synchrotron image of Zotefoams LDPE foam of nominal density 45 kg m^{-3} with 1 mm scalebar and (b) SEM image of EPS foam of density 19 kg m^{-3}.

which, expressed as fractions of the orthogonal lattice vectors of equal length a, are (0, 0, 0), (0.5, 0.5, 0.5) and their translational equivalents in the lattice. The foam structure was generated from a Surface Evolver representation (Brakke and Sullivan, 1997), in which the lattice vector is 2 units, so that the cell diameter D between parallel square faces is 1 unit. Fig. 1 shows the 'two cell high' model for [1 1 1] direction compression of the dry Kelvin foam, with height twice the cell diameter between hexagonal faces, or $0.5\sqrt{3}D$. A four-cell high model was also used. The prism corner coordinates and most vertex coordinates are given. The model boundaries, a prism of equilateral triangle cross-section with axis along [1 1 1], are mirror symmetry planes (Mills and Zhu, 1999).

If the model boundaries for [0 0 1] direction compression contain foam faces, it is difficult to impose suitable periodic symmetry conditions on such faces. Consequently the model used (Fig. 2) is that of Mills and Zhu (1999), quadrupled in height to be $2D$ high and contain 10 partial cells; its width and depth are $D/\sqrt{2}$. McKown (2005) used a similar model, but with twice the width and depth.

The intention was to study the foam collapse, and not the 'end-effects' of cut faces and open partial cells, near cut surfaces of the foam. Therefore incomplete cells, like cells 2 and 8 in Fig. 1, were closed by adding polymer faces on the prism top and base. These smaller end-cells respond slightly differently to complete cells, but the model response should be a reasonable approximation to that of a much thicker foam sample. Comparison of the responses of the 2-, 4- and 6-cell high models will indicate the height required for the effect of the smaller end-cells to be negligible. Small models risk excluding deformation patterns that occur in larger models; Gong et al. (2005) showed long-wavelength buckling occurred in tall open-cell Kelvin foam models compressed in the [0 0 1] direction, but not in small models. However, here cell faces are the only structural elements, and none of them lie in the lateral symmetry boundaries, so the deformation pattern should not depend on the symmetry conditions imposed on the model. As a check, a version of the [1 1 1] model, with twice the width, so containing four of the prisms shown in Fig. 1, was also analysed.

The dry Kelvin foam is a reasonable approximation to the structures of Zotefoam LDPE and EPS foams (Fig. 3) and the face thicknesses appear to be constant. The faces in the EPS foam are flat, but some in the LDPE foam are wrinkled. In the FEA models (Figs. 1 and 2), each trio of faces maintains their angular separations at the line-edge where they meet. In real polymer foams, three faces are similarly constrained by being joined to a narrow cell edge. The foam relative density R (Table 1) was varied over the commercial range by using four values of the (uniform) cell face thickness; R was calculated from the face area in the model (Fig. 1), ignoring the end faces added to complete cells, and including only one of the 'real' faces at the model ends. R was kept below 0.08, as foams with higher values have more complex microstructures than the dry Kelvin model.

Attempts to consider a wet Kelvin foam, with edge regions of finite extent modelled by continuum solid finite elements, have, at present, failed.

2.3. Modelling air-filled cavities in ABAQUS

For efficient FEA, the air phase, which makes up more than 90% of the foam volume, is better represented by a fluid cavity surrounded by a closed surface, than by multiple 3D elements. Dynamic FEA in ABAQUS supports 'surface-based fluid cavities', which can be gas or liquid filled. However the pre-processor ABAQUS-CAE, used to prepare the input file of model geometry and properties, does not support such cavities. Therefore an input file, generated using CAE, was edited to add the fluid cavities. The boundary symmetry planes of the model (Figs. 1 and 2) cut all the cells, and the surfaces surrounding each fractional air-cell (fluid cavity) include two symmetry planes. As the examples in the ABAQUS manuals do not show the use of symmetry planes across surface-based fluid cavities, trial and error was used to find the correct locations in the input file to insert the additional information (see Appendix).

The symmetry planes were modelled by *surface elements* (elements with zero in-plane modulus), which cannot be allocated mass. In dynamic FEA, the displacement of zero-mass elements must either be zero (encastre), or constrained to equal that of a finite-mass element, to avoid infinite accelerations.

In the ABAQUS jargon, the Kelvin model 'assembly' consisted of several 'parts': the polymeric foam, the symmetry surfaces, a rigid flat table at the base, and a flat-faced rigid striker. Each air-cell surface (such as that shown in Fig. 4) was defined using the relevant faces of the polymer 'part'. It was then redefined, with the same name, in the 'assembly', adding the appropriate pair of symmetry surfaces to complete a closed surface. The symmetry surfaces can be larger than strictly necessary to complete the closed cell. The air pressures on either side of the planar symmetry surfaces are equal, in the partial cell and in its mirror-image extension.

Table 1
4-Cell high Kelvin model, for foams of cell diameter 1 mm

Face thickness (μm)	Foam relative density (R)	LDPE foam density (kg m^{-3})	EPS foam density (kg m^{-3})
7	0.0234	21.6	24.6
10	0.0335	30.8	35.1
14	0.0467	43.1	49.2
22	0.0736	67.8	77.3

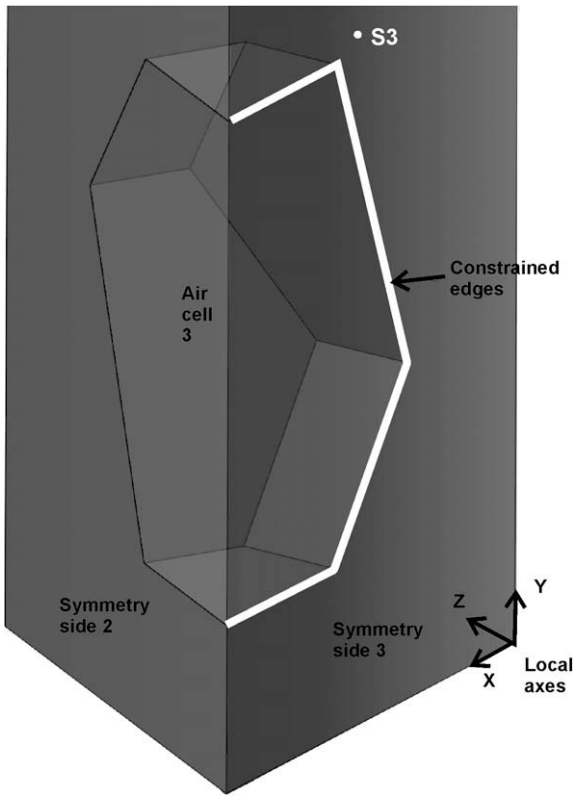

Fig. 4. A cell boundary in the model consists of polymeric faces plus two symmetry planes, with local normals *z*. S3 is a control point on side plane 3.

Although the air-cell boundaries consisted of both deforming polymer surfaces and non-deforming symmetry surfaces, each cell remained sealed, and the contained air mass was predicted to remain constant. ABAQUS calculates the cavity air mass m_C from the gas molecular mass M and the cavity volume V_C using

$$m_C = \frac{V_C M p_a}{R_0 T_0} \tag{2}$$

where R_0 is the gas constant, T_0 is the absolute reference temperature (equivalent to 0 °C) and p_a the absolute pressure in the cells at the start of the simulation. The air specific heat at constant pressure was given an arbitrary high value, so that the value at constant volume does not become negative.

2.4. Symmetry boundary conditions

The boundary conditions on the side surfaces of the [1 1 1] direction model are illustrated by reference to Fig. 4. The three mirror symmetry surfaces have local *z* axes along their normals. In variants of the model three side symmetry surfaces were:

(a) encastre, for the zero Poisson's ratio assumption.
(b) free to move along their *z* axes. Each was constrained so its local U*z* displacement equalled that at its midpoint (S1 for surface 1). A further U*z* coupling constraint occurred between S1 and the edges of the polymeric structure that lay in the symmetry plane. Two constraint equations stated that the local Uz displacements of S1, S2 and S3 were equal.

Section 4.1 shows that variant (a) produced faster run times than variant (b).

Cell faces, where they meet a side-symmetry surface, must maintain their initial perpendicular orientation; to achieve this, a boundary condition stated that the appropriate edges of these faces had rotations $UR_x = UR_y = 0$.

At large foam deformations, the cell faces must not interpenetrate; the 'general contact' option in ABAQUS 6.7 (2007) was selected for each air-cell surface, using frictionless surface contact with separation allowed, and penalty contact conditions.

2.5. Material properties

The mechanical properties of polyethylene depend on its crystallinity and crystal orientation, and on the strain rate (Mills, 2005). Almanza et al. (2005) showed that the crystal orientation in cell edges in LDPE foams differs from that of the cell faces.

Since single cell faces are too small for direct measurement of mechanical properties, Mills and Zhu (1999) measured the properties of 6.5 times biaxially drawn polyethylene film of the same crystallinity (density 920 kg m^{-3}) as the LDPE foam tested. Tensile tests at strain rate 7×10^{-4} s^{-1} gave a Young's modulus $E = 200$ MPa. Their engineering stress–strain data was converted to true stress versus true strain. The stresses were then increased by 20%, because of the viscoelastic nature of LDPE, to be appropriate for a strain rate of circa 50 s^{-1}. The data (Fig. 5) was fitted with a bilinear relationship, using an initial true yield stress $\sigma_Y = 12$ MPa, increasing linearly to 18 MPa at a true plastic strain of 0.26, and to 48 MPa at a true strain of 0.67. The parameters used for 5.5 times biaxially drawn PS in the glassy state were $\rho = 1050$ kg m^{-3}, $E = 3.0$ GPa. The true stress strain graph (Fig. 5) was fitted with $\sigma_Y = 73$ MPa which remained constant at higher strains. The material properties were taken as strain rate independent.

2.6. Modelling compressive impact tests

In falling-mass impact compression tests, the stress can be measured at the impacted top surface, or at the static base surface, of a foam specimen. To predict both stresses by FEA, the model loading conditions imitated those in the test. A 'rigid'

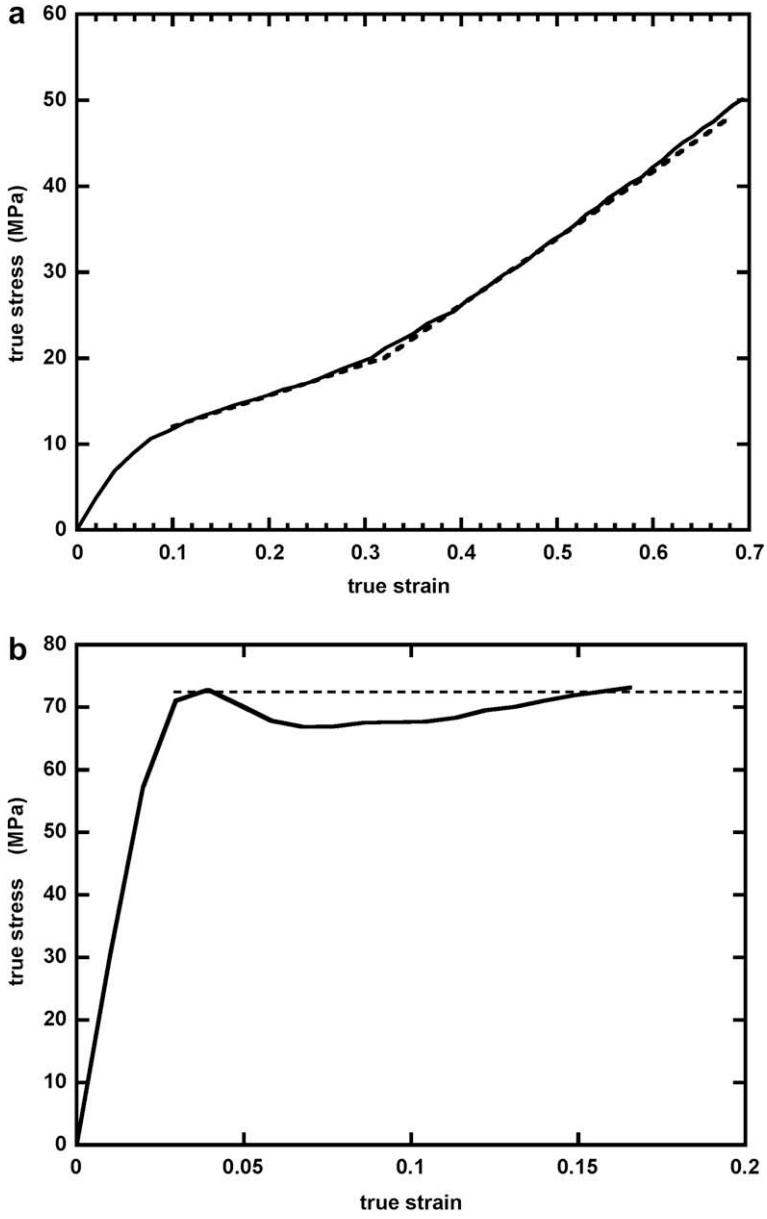

Fig. 5. Tensile true stress vs. true strain curves for biaxially oriented LDPE and PS films, converted from Mills and Zhu (1999) data. The approximations used in the FEA model are shown as dashed lines.

flat-faced striker of mass m_S was given a pre-impact velocity that imposed the required mean true strain rate, for example, for a 4-cell high model $V_1 = V_2 = V_3 = 86$ mm s^{-1} gave an engineering strain rate of 43 s^{-1} initially, which decreased during loading, and an initial true strain rate of the same magnitude, which increased during loading and averaged circa 50 s^{-1}. As the 4-cell high [1 1 1] direction model was 3.46 mm high with cross-section area 0.288 mm^2, the striker mass was chosen in the range 0.2–50 g, depending on the foam density, polymer and mean strain rate, to achieve peak compressive engineering strains circa 70%. Frictionless kinematic contact with no separation was assumed between the model base and the rigid flat table. The striker contact at the top of the model was frictionless with separation allowed.

The initial cross-sectional area of the [1 1 1] model was $0.5/\sqrt{3}\,D^2$ for cell diameter D, while the axial compressive force on the model base was $\sqrt{3}$ RF$_1$ and $\sqrt{3}\,m_S\,A_1$ on the model top. RF$_1$ is the support table reaction force component, and A_1 is the striker linear acceleration, in the 1 direction. Consequently, the engineering stresses on the model top and base could be calculated (engineering stresses and strains were used unless otherwise stated).

The initial height of the 4-cell high [1 1 1] model was $2\sqrt{3}\,D$ so the mean axial compressive engineering strain in the foam e_C was related to the displacement U_1 of the model top by

$$e_C = \frac{U_1}{2D} \tag{3}$$

The residual strain after impact could be predicted, as the model was free to expand in height once the striker rebounded from its upper surface. The foam lateral strain e_L was calculated from the lateral displacements of the symmetry boundary planes, ensuring that small lateral displacements of the whole prism did not affect the result.

The air pressure contribution σ_{TA} to the stress on the top of the [1 1 1] model was calculated from the relative air pressures in cells 1–3, allowing for their relative top areas (Fig. 1 shows the numbering), using

$$\sigma_{TA} = 0.4062(p_1 + p_2) + 0.1875p_3 \tag{4}$$

σ_{TA} was subtracted from the stress on the model top, to give the polymer contribution σ_{TP} to the top stress.

2.7. Meshing, mass scaling and subsidiary analyses

Checks were made that the mesh size did not affect the predictions. Meshing used a global seed size of 0.03 (30 μm for a 1 mm diameter cell), with 9772 triangular linear shell elements S3R for the cell faces in the 4-cell high [1 1 1] direction model, 3248 linear quadrilateral surface elements (SFM3D4R) in each symmetry surface, and 784 rigid triangular units R3D3 in each of the support table and striker. The Simpson integration rule was used to evaluate the shell properties, using five integration points through the thickness. The large deformation option was used.

The Surface Evolver model of the Kelvin foam has a cell diameter $D = 1$, while the material parameters for ABAQUS must have consistent units (not part of the input file). Since the foams being modelled have cell diameters typically in the range 0.1–1 mm, the simulations used $D = 1$ mm.

The ABAQUS manual suggests the use of (t mm s) units, with forces in N, dimensions in mm, densities in t mm^{-3}, and Young's modulus and yield stresses in N mm^{-2}or MPa, as an alternative to SI units. The Surface Evolver model was used with these units, so $D = 1$ mm. For quasi-static problems, mass scaling is an accepted method of reducing the run time. Increasing the polymer density by a mass scaling factor f increased the critical time step by a factor $\sqrt{f}$ and reduced the run time by a factor that was nearly as great. For post-yield simulations at strain rate 50 s^{-1}, $f < 100$ could be used without changing the foam stresses or deformation mechanisms. However, the pre-yield response becomes increasingly noisy if $f > 10$, so the smallest value consistent with reasonable run times was used to predict the initial yield stress.

To check on the use of fluid filled cavities and mass scaling, a simple structure, consisting of four, prism-shaped cells in series, was analysed. The cell 'faces' lay in planes perpendicular to the compression axis, so these did not resist the compression of the model, which depends entirely on the 'air-spring' cells. The expected isothermal air compression response was predicted.

A quasi-static reference result would be ideal to judge the strain rate contribution to the foam impact response. However gas-filled cavities cannot be used with static (implicit) FEA. Therefore dynamic FEA was performed at lower strain rates, for reference purposes.

3. Experimental methods

3.1. Drop impact tests

These tests were performed at EMPA, St Gallen. A vertically falling, flat-faced steel block of 5 kg, instrumented with a Kistler 5000 g quartz accelerometer (Type 8005) was used to strike the samples, supported on a flat-faced table. A Kistler quartz force transducer of 60 kN capacity (Type 9361B), below the table, was used to detect the impact force. The sensor signals were amplified with two Kistler charge amplifiers (Type 5011B) and sampled at 100 kHz with a Nicolet BE490XE transient recorder plug-in board. To prevent aliasing and suppress eigenfrequencies, a 2-pole Butterworth low-pass filter with a cut-off frequency of 3 kHz was selected with the Kistler amplifiers. Numerical integration of the acceleration was used to compute the compressive strain in the foam.

3.2. Poisson's ratio measurements

Slow compression tests with lateral strain measurement, as described in Chapter 5 of Mills (2007a), were performed on foam samples that were approximately a 25 mm cube.

3.3. X-ray CT structure analysis

Synchrotron radiation X-ray tomographic microscopy (SRXTM) data were collected at the beamline for TOmographic Microscopy and Coherent rAdiology experimenTs (TOMCAT) (Stampanoni et al., 2006) at the Swiss Light Source (SLS). The 3D Zotefoams LDPE structure was reconstructed from 1000 projections acquired at a photon energy of 8 keV and with an exposure time of 550 ms (per projection). The voxel size was approximately 11 μm.

4. Results

4.1. Initial results, and choice of model

The influence of the mass scaling factor f was investigated for the 2-cell high [1 1 1] model at a strain rate of 50 s^{-1}, with free lateral expansion allowed. An increase in f from 1 to 10 produced occasional minor oscillations in the stress–strain curve (Fig. 6), but no change in the initial yield stress σ_0, which was defined as the initial stress maximum; this corresponded to the first coordinated plastic buckling of three connected cell faces, and the partial collapse of three cells. Low energy impacts were used to impose maximum foam strains less than 5%; although the stress–strain response was non-linear (shown later to be due to elastic buckling of cell faces), there was complete recovery of foam dimensions on unloading, and no material yielding. An increase in f from 10 to 100 caused an artificial 5% increase in σ_0 (Table 2) so $f = 10$ was used to predict the low strain response and σ_0. The response at strains >0.2 was predicted using $f = 100$, to avoid excessive run times (Table 2); the influence on the stresses in this region was minor. For predictions of the residual strain after unloading, it was possible to use $f = 1000$.

The initial yield stress of the 6-cell high, free lateral expansion, model (Table 2) was within 3% of those in the 4-cell and 2-cell high models, while the pre-yield responses were identical. The post-yield drop in foam stress, due to the collapse of three cells, was partly driven by air pressure decreases in other cells, and elastic recovery of faces. A related phenomenon, the stress drop when a neck forms in a long polyethylene tensile test specimen, is also driven by elastic unloading of unyielded material. The cell pressure rise was sudden in the 4-cell (Fig. 7) and 6-cell high PE foam models. In the 2-cell high PE foam model, and the 4-cell high model of EPS foam of the same density (Fig. 7), the pressure rises in the collapsed cells were more

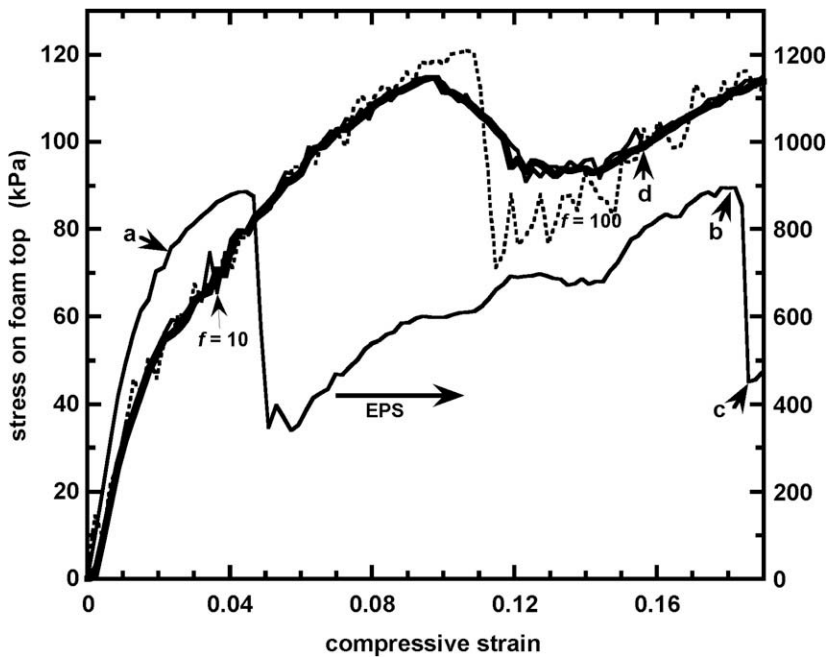

Fig. 6. Effect of mass scaling factor f on stress strain response of 2-cell high [1 1 1] models of LDPE foam of density 43 kg m^{-3}: thick solid curve for $f = 1$, thin solid curve for $f = 10$. The scaled response of EPS of density 49 kg m^{-3} (4 high model, free expansion, $f = 10$) is included for comparison. The geometry of states a, b, c, and d are shown in Fig. 13.

Table 2
43 kg m^{-3} density LDPE foam models compressed in the [1 1 1] direction

Model height cells	Mass scaling factor	Strain rate (s^{-1})	Initial yield stress σ_0 (kPa) (run time in hours for 50 ms)	
			$\nu = 0$	ν free
2	1	50	122 (7.2)	115 (100)
2	10	50	119 (2.3)	115 (33)
2	100	50	116 ± 2 (0.7)	121 (10.7)
4	1	50	123 (10)	
4	10	50	120 (3)	118 (225)
4	10	5	114 (3)	
6	1	50	123 (4.4)	
6	10	50	117 ± 1 (1.4)	
6	100	50	115 ± 5 (0.4)	115 ± 3 (235)

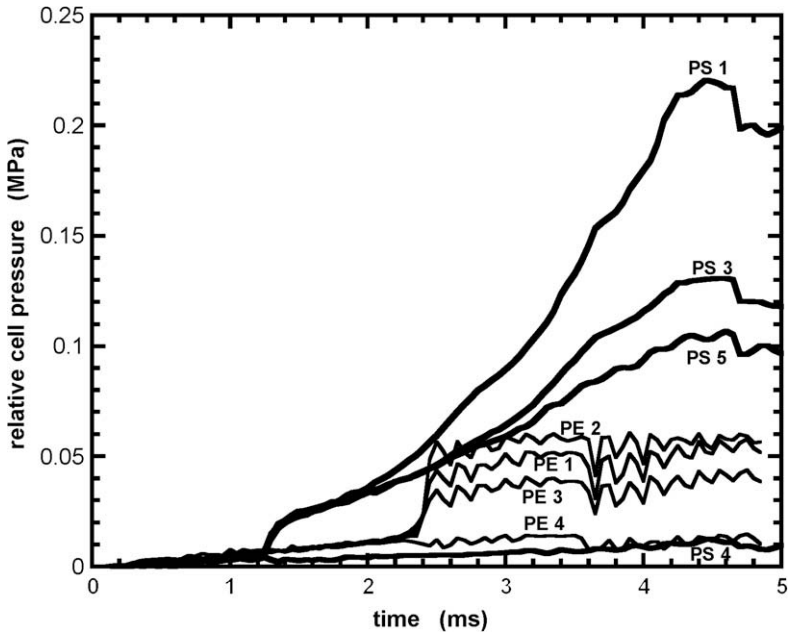

Fig. 7. Pressure histories for cells 1–4 in 4-cell high [1 1 1] models of 43 kg m^{-3} density PE foam, and cells 1, 3, 4 and 5 in 49 kg m^{-3} PS foam, compressed at strain rate 50 s^{-1}.

gradual. Elastic energy release, from unloading other parts of the model, was sufficient to complete the face plastic buckling in the 4-cell high PE foam model. However, elastic energy release was insufficient in the stronger EPS foam model, so plastic face buckling required further energy supply from the kinetic energy of the striker.

For the 2-cell high [1 1 1] model, a decrease in strain rate from 50 to 5 s^{-1} caused only a 5% reduction in σ_0, showing that both predictions are effectively quasi-static results. If, however, the polymer properties had been taken as strain rate dependent, the predicted foam properties would be strain rate dependent.

Allowing the model to expand laterally caused a 6% reduction in the initial yield stresses, but large increases in run time (Table 2), compared with a zero Poisson's ratio condition. The run times were excessive for the 6-cell high model for mass scaling factors $f < 100$, while those for EPS simulations were four times larger than for PE foams, due to the higher Young's modulus of polystyrene. Consequently, all subsequent predictions for [1 1 1] direction compression are for 4-cell high models, with lateral expansion allowed, using $f = 10$ for the low strain response, and $f = 100$ for the high strain response.

4.2. Kelvin foam model, compressed in the [1 1 1] direction

4.2.1. Stress–strain relationships

Impacts on LDPE foam were simulated for a mean true strain rate of 50 s^{-1}, a typical strain rate for compressive impact tests Small cell pressure oscillations at a frequency circa 16 kHz were predicted (Fig. 7), while three cell pressures increased suddenly by circa 40 kPa when the intervening faces buckled plastically. Over the 50 ms of impact, with pressures rising to circa 1 MPa, all the cells had nearly the same pressure versus time relationship. Hence, before yield, and after all the cells

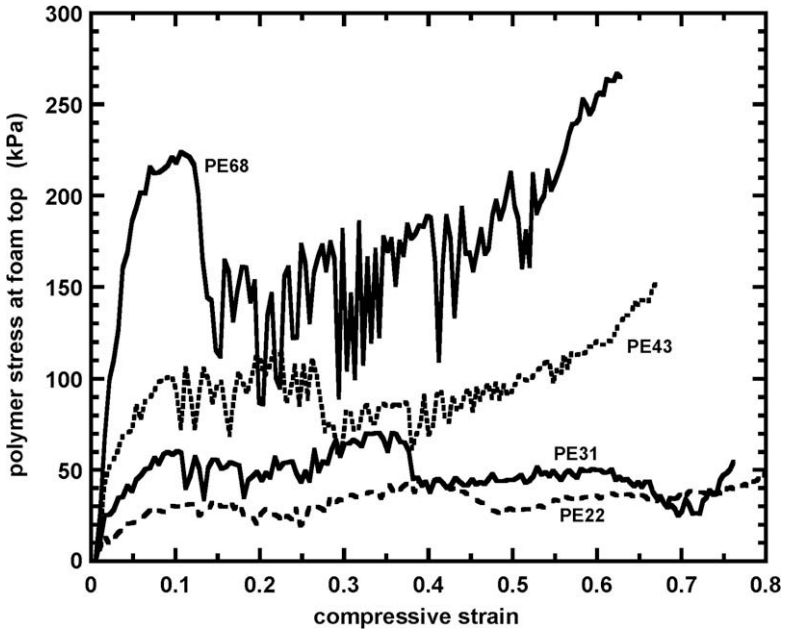

Fig. 8. Polymer contribution to the stress on the model top, for LDPE foams of the densities (kg m^{-3}) labelled.

have started to collapse, the cell deformation is nearly homogeneous. The stress acting on the top of the specimen was predicted to be within a few % of that on the base.

Fig. 8 shows that σ_{TP}, the polymer contribution to the stress at the model top, was nearly independent of compressive strain in the range 0.1 (the initial yield strain) to 0.6 (before face-to-face contact occurs). The mean and standard deviation of σ_{PT} were evaluated over this strain range (Table 3). Sudden falls in σ_{TP}, due to localized elastic unloading, increased in magnitude with foam density; more elastic energy was stored in the deformed polymer in denser foams. For the higher foam densities, σ_{TP} increased at strains >0.6, and for the lower densities, at strains >0.7.

Fig. 9 shows that the experimental stress, for Zotefoams LDPE foam of nominal density 45 kg m^{-3}, is about 20% higher than the prediction of the FEA model at the same strain. This difference could be removed by using 20% higher yield stresses for the LDPE in the FEA input. Above 500 kPa, the stress rose steeply to a peak then dropped almost instanteously on unloading. The position of the unloading curve depended on the impact energy density; that chosen for the FEA simulation produced a maximum strain of 0.883, while the experimental maximum strain was 0.85. The cell air volumes were calculated without allowance for the face thickness, so, for this aspect alone, the volume fraction of cell air in the foam was 1.0. Hence in Eq. (1) $R = 0$, so the mean cell pressure should be proportional to $\varepsilon/(1\text{-}\varepsilon)$. Such a plot for a zero Poisson's ratio model showed this to be the case, for the 50 s^{-1} strain rate; the constants of proportionality, 98.6 and 97.9 kPa for densities 22 and 69 kg m^{-3}, respectively, were close to the input atmospheric pressure p_0 of 101.3 kPa. Hence the dynamic cell air compression at a mean strain rate of 50 s^{-1} was the same as the static compression, used to derive Eq. (1).

The lateral expansion in compressive impact tests was predicted to be less than 1% at 30% compressive strain (Table 3). Predictions for EPS of density 25 kg m^{-3} are compared with lateral expansion data, determined in a slow compression test, in Fig. 10. The very small lateral expansions were similar pre-yield; the predicted expansion increased after the compressive yield point, but remained very small.

Table 3
Predictions of the 4-cell high Kelvin model, for foam cell diameter 1 mm, compressed along [1 1 1] at nominal strain rate 50 s^{-1}, with free lateral expansion

Polymer	Foam density (kg m^{-3})	Initial yield stress σ_0 kPa	Polymer stress σ_{PT} for 0.1 < e_c < 0.6 kPa (± std. dev.)	Lateral strain when e_c = 0.3 (%)
LDPE	21.6	46	33 ± 6	0.3
LDPE	30.8	74	51 ± 9	0.7
LDPE	43.1	118	93 ± 14	1.0
LDPE	67.8	240	173 ± 39	1.2
EPS	24.6	310	250 ± 50	0.5
EPS	35.1	550	420 ± 110	0.5
EPS	49.2	890	680 ± 150	1.0
EPS	77.3	1810	1560 ± 230	1.9

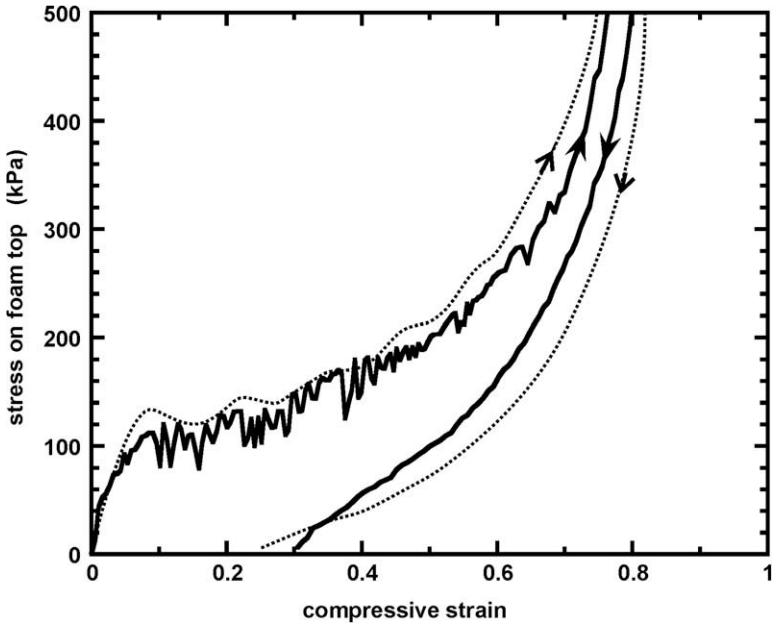

Fig. 9. Stress strain curves for impact loading and unloading LDPE foam of density 43 kg m^{-3}: solid curve [1 1 1] 4-cell high FEA model, dotted curve experimental data.

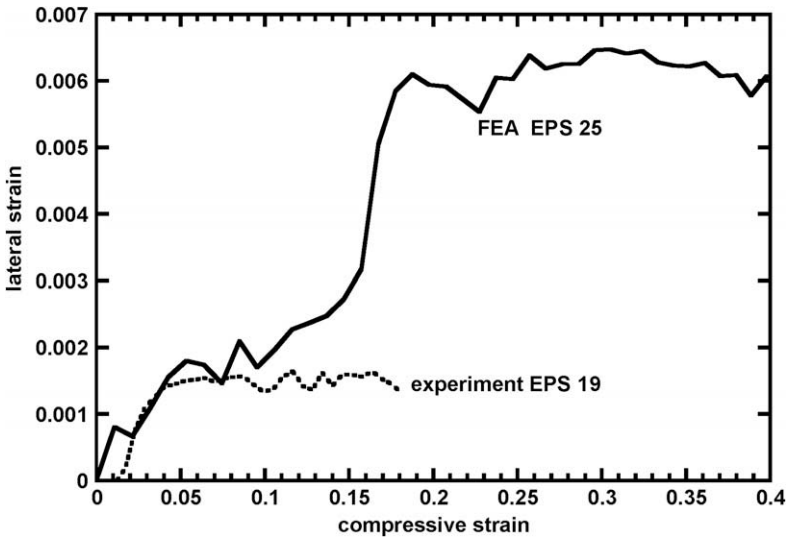

Fig. 10. Lateral strain vs. compressive strain for EPS foams: FEA for impact of density 25 kg m^{-3}, experimental data for slow compression of density 19 kg m^{-3}.

Increasing the polymer Young's modulus from 200 to 300 MPa caused the initial compressive yield stress of LDPE foam of density 43 kg m^{-2} to increase by 8%, showing that the foam yield stress was mainly determined by the yield stress of the oriented LDPE faces. As the yield stress of the LDPE was assumed to remain constant, the decreased yield strain, hence reduced amplitude of cell face elastic buckling, reduced the softening effect of geometry change prior to yield. The initial yield stress (kPa) versus LDPE foam density ρ (kg m^{-3}) relationship, on logarithmic scales (Fig. 11a), followed the power law

$$\sigma_0 = 0.554\rho^{1.443} \tag{5}$$

with a correlation coefficient $r = 0.9993$. The predicted initial yield stresses are about 20% lower than experimental impact values (Ankrah, 2003) for Zotefoams LDPE foams, with the difference being greatest at low densities. This suggests again that the tensile yield stress of the LDPE, used in the FEA, should have been 20% higher.

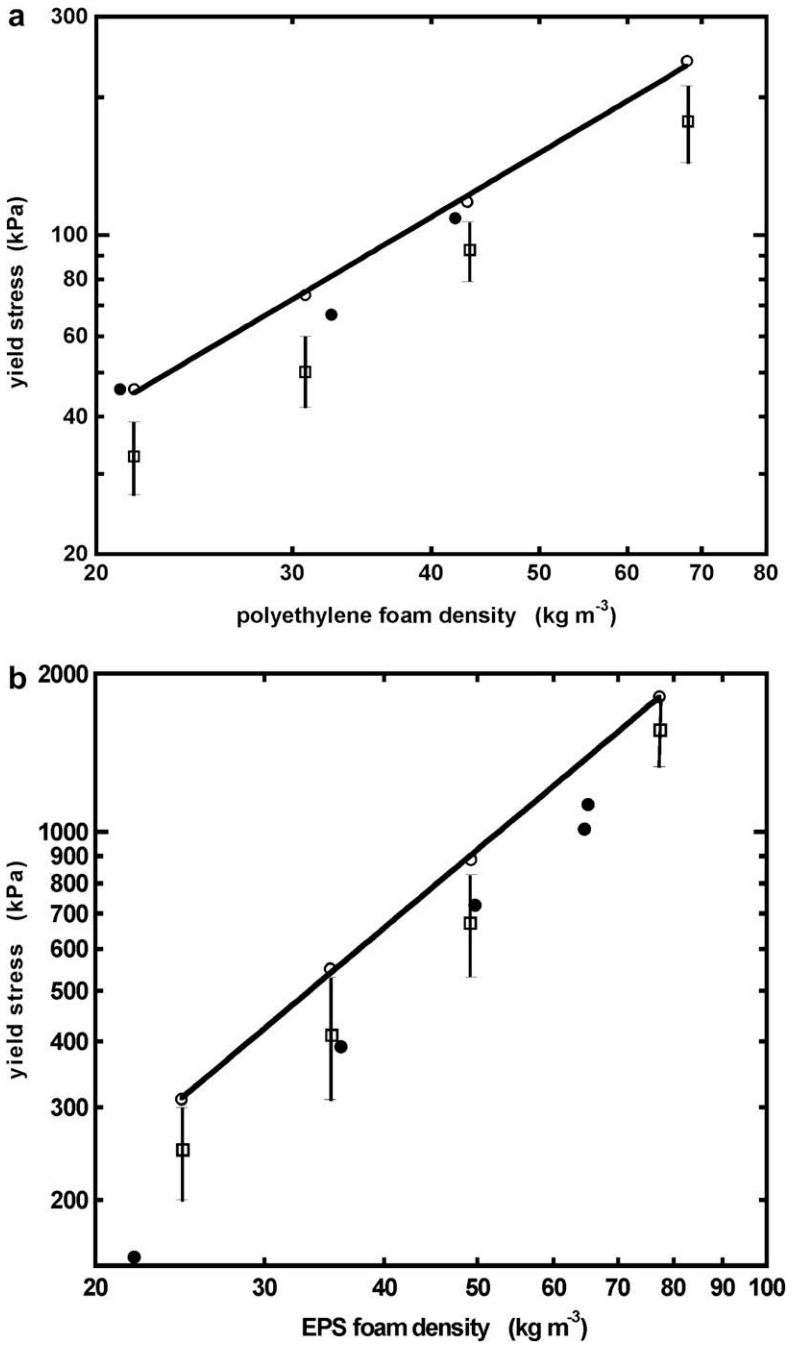

Fig. 11. Initial yield stress (open circles), mean and standard deviation of σ_{PT} (squares with vertical lines) compared with experimental data (solid circles) vs. density: (a) LDPE and (b) EPS foams.

The variation in initial yield stress (kPa) with EPS foam density (Fig. 11b) could be described by

$$\sigma_0 = 2.316\rho^{1.532} \tag{6}$$

with a correlation coefficient $r = 0.9999$. Experimental data (Mills, 2007a) lies below the predictions, but closer to the mean value of σ_{PT}. The predicted lateral strains are slightly larger than those of LDPE foams of the same density.

Predicted residual strains for EPS of density 49 kg m^{-3} increased with the maximum foam strain in an impact, but were somewhat larger than experimental data for EPS of density 65 kg m^{-3} (Mills, 1996) (Fig. 12). However, the predicted residual strains for LDPE foams were much lower; experimentally there is almost complete recovery.

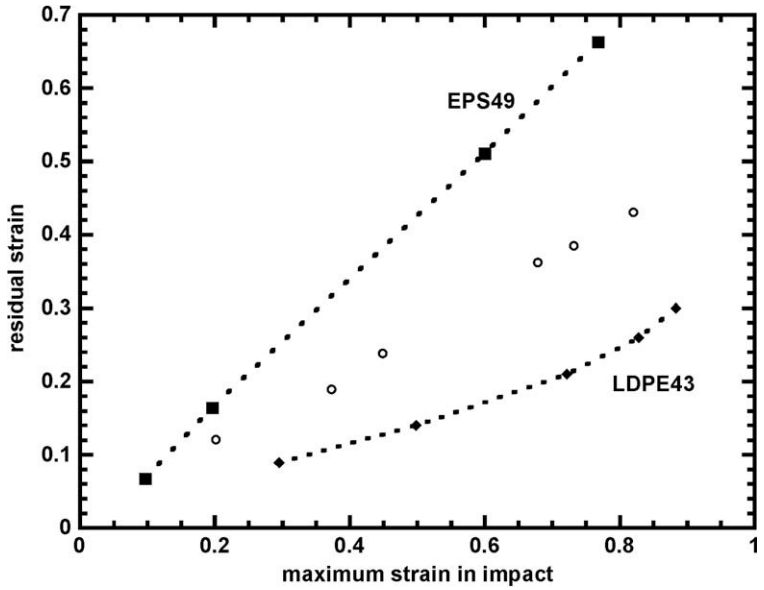

Fig. 12. Residual strain vs. maximum impact strain, predicted using the 4-cell high [1 1 1] model for foams (density labelled) impacted at 50 s^{-1}, compared with experimental data for EPS of density 65 kg m^{-3} (circles).

Table 4
Predictions of 4-cell high Kelvin model, for foam cell diameter 1 mm, compressed along [1 1 1] at nominal strain rate 500 s^{-1}, with free lateral expansion

polymer	Foam density (kg m^{-3})	Initial yield stress, σ_0 (kPa)	Increase c.f. 50 s^{-1} (kPa)
LDPE	43.1	122 ± 2	4 ± 2
EPS	49.2	890 ± 10	0 ± 10
EPS	77.3	1880 ± 30	70 ± 10

When the nominal strain rate for foam impacts was increased from 50 to 500 s^{-1}, the initial yield stresses did not increase significantly (Table 4), nor did the amount of softening after yield increase. Hence, there were no micro-inertial phenomena observed of the type described by Deshpande and Fleck (2000).

4.2.2. Deformation mechanisms

In the model of EPS foam of density 49 kg m^{-3} hexagonal cell faces buckled elastically into sinusoidal shapes before the foam strain reached 1%, while square faces assume domed shapes. The direction of buckling of some square faces reversed above 1% foam strain, reducing cell pressure differentials. The stress–strain curve is non-linear prior to yield (Fig. 6), due to this elastic buckling. At 2.6% foam strain (Fig. 13a) the initial plasticity, revealed by contours of the equivalent plastic true-strain PEEQ, was face stretching near a vertex. The first collapse was at the top of the model, involving two smaller-volume cells, so the second collapse, involving full-sized cells, is described. Pairs of *plastic hinges* formed across a pair of linked hexagonal cell faces (Fig. 13b), at 890 kPa stress. The formation of a pair of plastic hinges across the neighbouring square face allowed the hexagonal face 'hinges' to rotate further, and the three faces to concertina while the stress fell to 450 kPa (Fig. 13c). The volumes of the bounded cells decreased while their pressures increased by about 120 kPa. Plastic strains up to 0.5 occurred as the folded faces bent over each other near the vertex. At higher foam strains, further sets of cells underwent similar pressure increases as the intervening faces buckled plastically, until, at 55% strain, all but the horizontal faces had concertinaed.

FEA predicted nearly the same cell collapse mechanism in LDPE foams. However the plastic hinges across the hexagonal faces were broader, while the square face stretched near the face junction (Fig. 13d) before forming a single broad plastic hinge; the pressure increase when the three cells partly collapsed was only about 40 kPa. All the cells had started to collapse by the time the foam strain was 40%. The 9.5% yield strain of the LDPE foam was roughly double that of the EPS foam (Fig. 6). At a foam strain of 88% (Fig. 13e) many face-to-face contacts had occurred. In a [1 1 1] model of twice the regular width, the same deformation mechanisms were observed around the four vertices at the same height; therefore the mirror symmetry boundaries do not affect the predicted deformation pattern. Even for LDPE foam of density 22 kg m^{-3}, plasticity was predicted to occur.

The polymeric contribution to the stress only rose, hence face-to-face touching only contributed to hardening, for strains >0.75 for 49 kg m^{-3} density EPS. Experimental drop-impact data for EPS of density 50 kg m^{-3} (Stauffer, 2007) showed stress

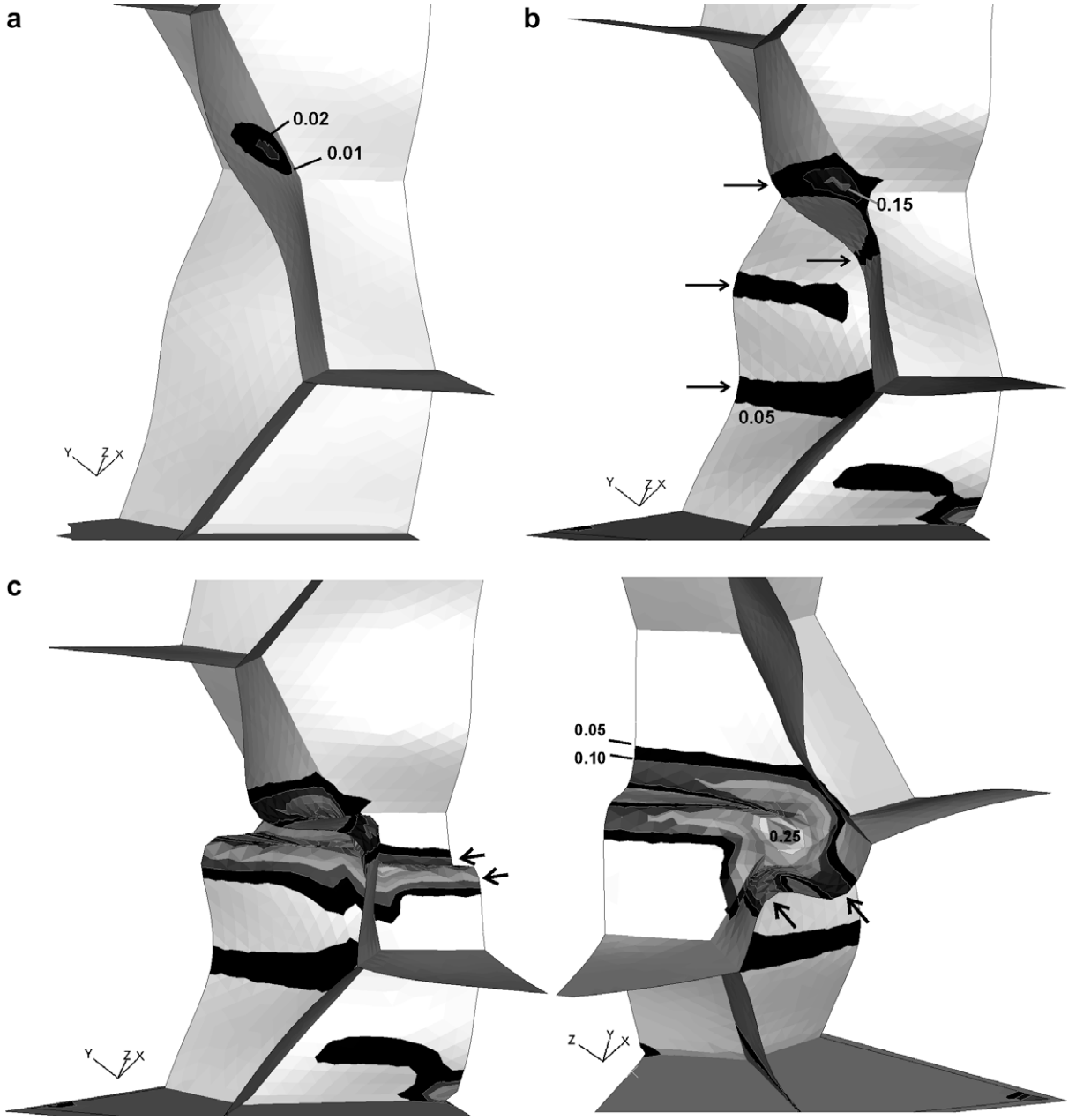

Fig. 13. Part of 4-cell high [1 1 1] models, with compression direction vertical. EPS of 49 kg m^{-3} density: (a) initial plasticity at 2.6% strain, (b) two plastic hinges (arrowed) in hexagonal faces, (c) two views of coordinated folding when two plastic hinges (arrowed) form in the square face. PE foam of 49 kg m^{-3} density: (d) similar stage to (c) with hinges or developing hinges arrowed, (e) face contact at 88% strain. Contours levels are plastic strain PEEQ. Points a to d are shown in Fig. 6.

increases in the strain range 0.1–0.6. If the predicted responses were heavily smoothed, they would agree quite well with experimental data (Fig. 14).

Two or three plastic hinges were visible across most cell faces in the unloaded foam model (Fig. 15a). Similarly folded faces were observed by SEM in EPS foams after compressive impact (Fig. 15b), although it was difficult to find coordinated folding of neighbouring faces.

4.3. [1 1 1] compression of Kelvin foam with initially wrinkled faces

Synchrotron images of Zotefoam LDPE foam showed the larger cell faces were slightly wrinkled (Fig. 3a), while some small faces appeared flat. Face bowing was induced in a Kelvin [1 1 1] foam model, by imposing different thermal strains

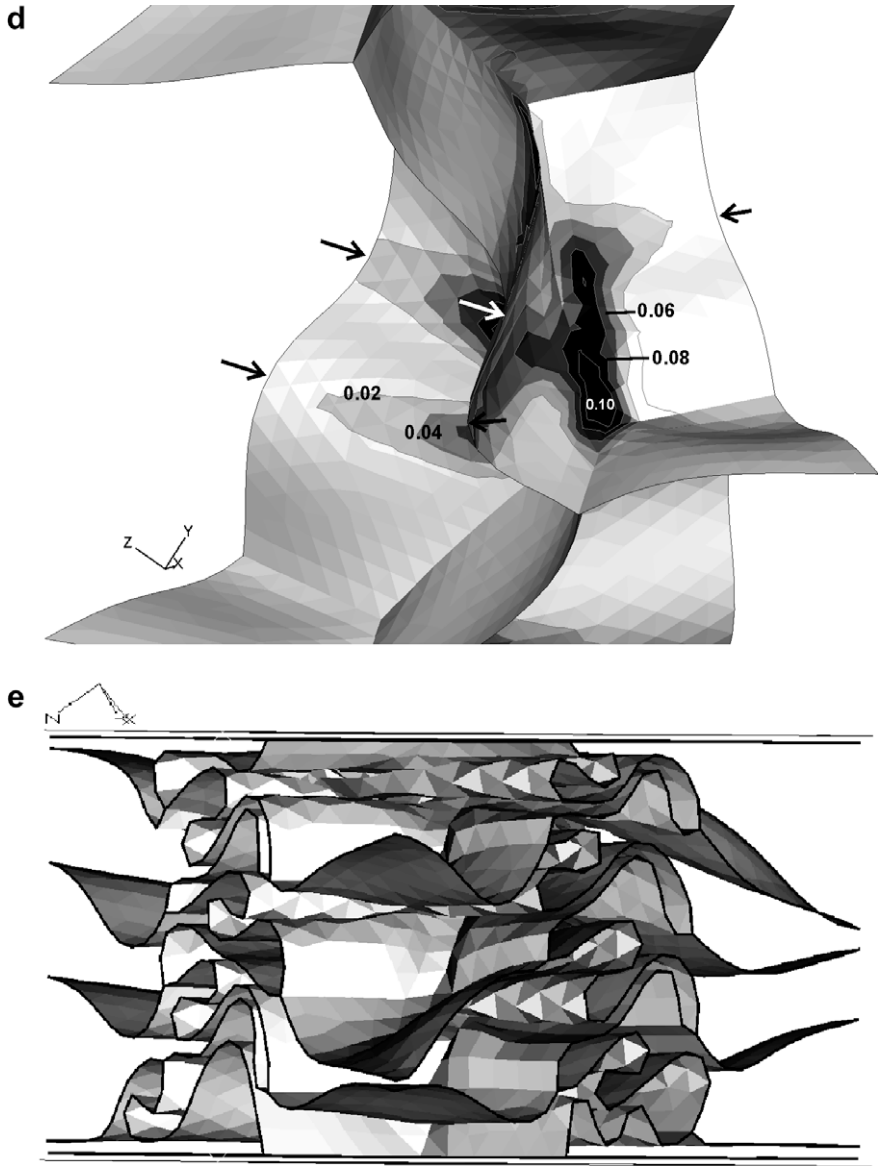

Fig. 13 *(continued)*

in the square faces (a contraction of 6% in length) and the hexagonal faces (an expansion of 2.5% in length), during an initial step lasting 2 ms, with lateral expansion allowed. Fig. 16 shows the S-shaped elastically buckled hexagonal faces, in part of a 4-cell high model, after this step. The flat square faces contained significant tensile stresses, while there was a small amount of plasticity near their corners. The face shapes are not dissimilar to those in Fig. 13a, when a 5% compressive strain is applied to a foam with initially-flat faces. An impact at a nominal strain rate of 50 s^{-1} occurred in a subsequent step; the predicted initial yield stress of 105 kPa for a 43 kg m^{-3} density LDPE foam was 11% smaller than that of the equivalent model with initially flat faces.

4.4. Kelvin model, compressed in the [0 0 1] direction

A two-cell high Kelvin model (Fig. 2) was analysed for foams of cell diameter 1 mm, and nominal impact strain rate 50 s^{-1}, with free lateral expansion allowed. The initial collapse mechanism was related to that in the [1 1 1] model; four hexagonal faces, meeting at the vertex with coordinates 0, 3, 0, each formed pairs of plastic hinges then concertinaed in a coordinated way, with plasticity near the vertex. In the LDPE foam models, the same happened nearly simultaneously in faces meeting at vertex 0, 5, 0. In the EPS foam models, there was sequential collapse around vertices 0,3,0, 0,5,0 then 0,7,0. This collapse forced the connected, initially-vertical, square faces to bend then crumple.

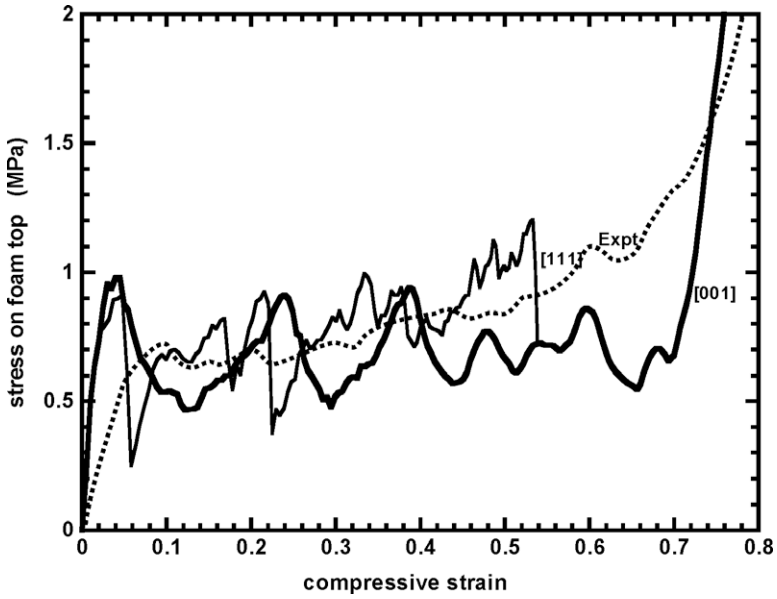

Fig. 14. Stress-strain responses of [001] and [111] direction models of 49 kg m^{-3} density EPS foam, compared with drop impact data (dotted curve) for density 50 kg m^{-3} (Stauffer, 2007).

For EPS of density 49 kg m^{-3}, the initial compressive yield stress of 0.97 MPa dropped almost immediately to about 0.5 MPa, then it oscillated between these levels for compressive strains <0.7 (Fig. 14). The initial yield stress, and mean polymeric contribution to the stress over the strain range 0.1–0.6, are given in Table 5. The anisotropy factor, defined as the initial yield stress for [001] compression divided by that for [111] direction, ranged from 1.01 to 1.09. Since a 2-cell high [001] model was compared with a 4-cell high [111] model, the Kelvin foam structure probably has an isotropic initial yield stress. The predicted lateral strains in the post-yield region were similar to those predicted for the [111] model. The half-size cells at the top and base of the [001] model were more stable than the complete cells; to reduce their effect, the model should be four or more cells high.

5. Discussion

The dry Kelvin model geometry is simple and its predictions are close to experimental data, although its face content (100%) exceeds that in LDPE foams (65–93%) and EPS foams (circa 95%). This shows that cell faces dominate the foam compressive response. In real foams the faces are slightly thinner at their midpoints than at their edges, but the modelling assumption of a uniform face thickness appears to be justified. The initial non-linearity of the stress–strain curve was shown to result from elastic buckling of faces, and 'pop-in' reversals of domed face curvature, rather than material yielding. However the polymer yield stress largely determined the predicted foam compressive response for compressive strains higher than 5%. The collapse mechanism in EPS, with pairs of plastic hinges across each collapsing face, is closer to an idealised 'paper-folding' mechanism than the mechanism in LDPE foams. This must partly explain the greater strain recovery after impact of LDPE foams. The FEA model supersedes Mills and Zhu's (1999) model of a Kelvin closed-cell foam compressed in the [001] direction, which unrealistically assumed a minimum 0.4 edge volume fraction, and overestimated the compressive stresses in EPS. Comparing FEA predictions at strain rates of 5, 50 and 500 s^{-1} showed that the initial yield stress did not increase with strain rate. Therefore the stress strain predictions can be compared with low strain rate data for EPS and LDPE foams, if allowance is made for polymer viscoelasticity. The model can be used in future to predict the performance of novel foams, with polymer properties or foam geometries that differ from those of well-established, low-cost foams. The major disadvantage of the model is the lack of variation in cell size, shape or orientation. This leads to sudden stress drops in 4-high or taller LDPE foam models, when the energy for the collapse of one layer of cells is provided by the elastic unloading of other layers. In the EPS foam models, relatively large stress falls were predicted post-yield. However in real polymer foams, the cells with the least favourable orientation will collapse first, while cell shape and size variations reduce the surrounding volume from which elastic energy can be released. The macroscopic foam stress, during foam crushing, averages the local stress on a cell-size scale, so varies less with compressive strain than does the FEA model.

The compressive yield stress of the Kelvin foam model was predicted to be nearly isotropic, as are LDPE foams produced by the Zotefoams nitrogen-expansion process and EPS. This is an advantage over other regular-cell models. The model is far less anisotropic than the open-cell wet Kelvin foam model (Mills, 2007a). The realistic compressive response, of small Kelvin closed-cell foam models, suggests that they include all the relevant deformation patterns, making it unnecessary to consider

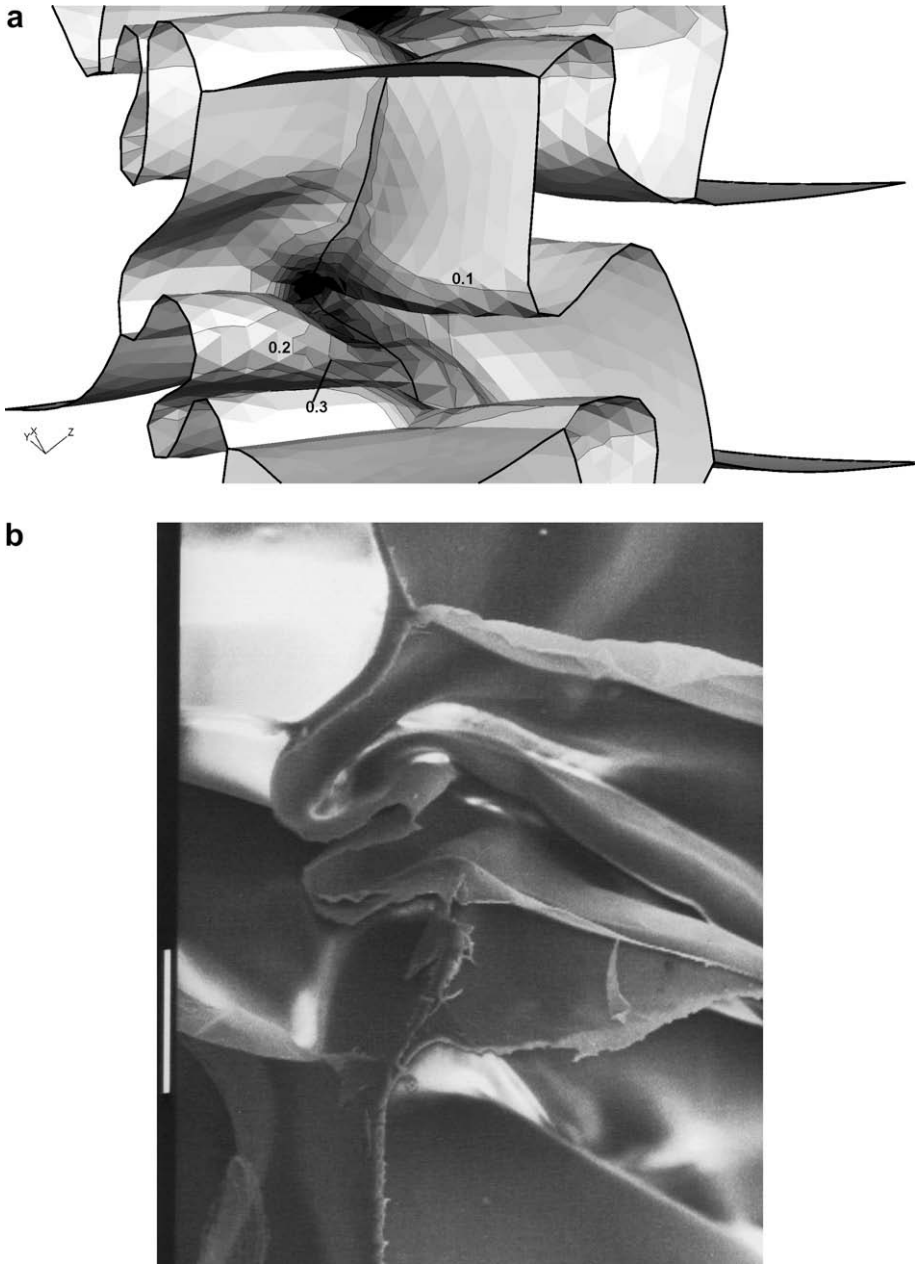

Fig. 15. (a) Contours of plastic strain PEEQ in unloaded 4-cell high [1 1 1] model of 51 kg m^{-3} density EPS foam, after impact compression to 0.77 strain, (b) SEM photo of EPS foam of density 35 kg m^{-3}, scale bar for 50 μm. Compression directions are vertical.

larger models. Increasing the height and width of the [1 1 1] direction model did not change the face deformation mechanism. In contrast, small open-cell Kelvin models (Zhu et al., 1997) showed insufficient stress–strain non-linearity when compressed in the [0 0 1] direction, but realistic non-linearity when compressed along [1 1 1].

The successful prediction of the foam compressive yield stresses suggests that the material modelling parameters, taken from slow tensile tests on biaxially stretched films, are reasonable estimates of the foam face properties. The material properties of LDPE, a semi-crystalline polymer, can change significantly with crystallinity and crystal orientation, as well as with strain rate. It may therefore be fortuitous that properties, taken from biaxially oriented LDPE film, give good predictions for LDPE foam. Recent reduction in the amount of butane blowing-agent in some EPS foams has increased the compressive yield stress by 10–20% at a given density, presumably by increasing the yield stress of the polystyrene.

The predicted power-law exponents of 1.44 (LDPE) and 1.53 (EPS) for the initial yield stress versus foam density relationships, are close to the experimental values of 1.44 for high density polyethylene foams (Mills, 1994), and 1.78 for EPS (Mills, 2007a). Santosa and Wierzbicki's (1998) foam deformation model, of three plastic hinges forming across each of four vertical

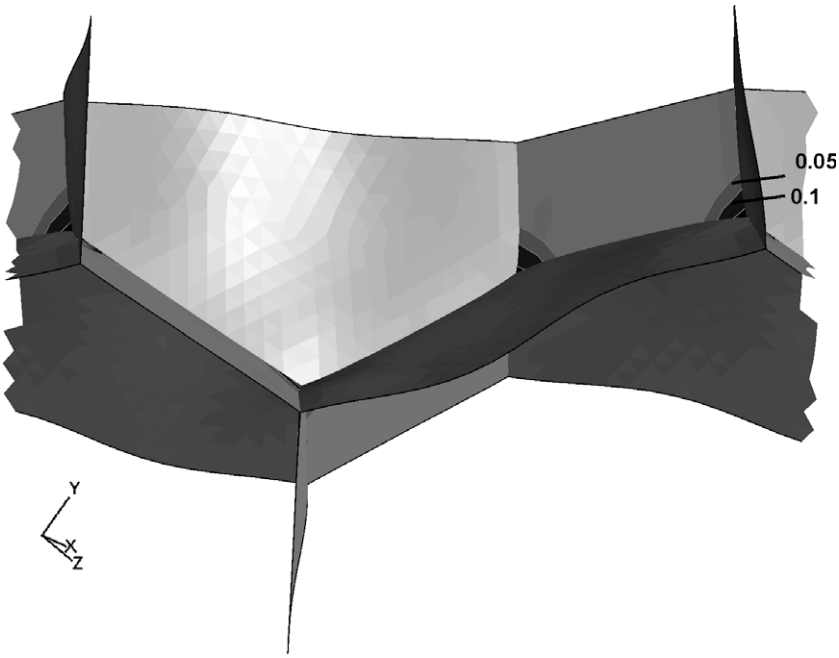

Fig. 16. Flat square faces and bowed hexagonal faces in part of a [1 1 1] Kelvin model, induced by differential thermal contraction. Contour levels of plastic strain PEEQ shown.

Table 5
Predictions for 2-cell high Kelvin model, with cell diameter 1 mm, compressed along [0 1 0] at initial strain rate 50 s^{-1}, with free lateral expansion

Polymer	Foam density (kg m^{-3})	Initial yield stress, σ_0 (kPa)	Yield anisotropy factor	Lateral strain when $e_c = 0.1$ (%)
LDPE	43.1	119	1.01	0.2
LDPE	67.8	242	1.01	0.6
EPS	49.2	970	1.09	0.2
EPS	77.3	1900	1.04	0.3

faces, and their coordinated plastic collapse, predicted compressive yield stresses that were proportional to the 1.52th power of foam density. Their collapse mechanism is related to the coordinated concertina collapse of linked faces in the dry Kelvin foam models. In contrast, Gibson and Ashby's (1997) qualitative model for the compressive collapse of closed-cell polymer foams assumed that cell edges dominated the response, and that these must form plastic hinges for the cells to collapse. To get their model to predict a power law exponent of 1.5, they claimed that the fraction of polymer in foam cell faces was low. However, this is contradicted by quantitative microscopy of low-density PE foams (Almanza et al., 2001). Their treatment of low density LDPE foams as collapsing elastically is also shown by the FEA to be unrealistic.

The polymer contribution to the compressive stress in LDPE and EPS foams was predicted to be almost independent of compressive strains $0.1 < \varepsilon < 0.6$, confirming that compressive stress increase is mainly due to cell air compression in this strain range. This validated Eq. (1) for LDPE foam.

Cell pressure differentials, by bowing the intervening faces, encouraged foam cells to collapse almost uniformly when compressed at drop-impact strain rates. However, the initial cell collapse proceeded inhomogeneously through the models, before nearly-uniform compression resumed for foam strains >0.5. This response differs completely from McKown's (2005) prediction, using a 2-cell high [1 0 0] model with no gas content, that face crumpling propagated from the top to the base of the foam. Mills' (1994) comment, that coordinated bellows-type deformation of neighbouring cell faces prevents pressure differentials developing between neighbouring cells, has been confirmed by the FEA. Face-to-face contact was predicted to occur at some locations, at foam strains $\varepsilon > 0.6$ (Fig. 6). This strain increased for lower foam densities, being >0.7 for LDPE foam of density 22 kg m^{-3}. This contact changed the mechanics of face deformation, causing the polymeric contribution to the foam stress to increase at high strains. The term 'densification' is inappropriate for this phenomenon, since the foam density increases throughout the compression.

It is realistic to treat EPS foam cell faces as being initially flat, but this is a simplification for LDPE foams. The wrinkled faces observed in the latter must form when the foam cools; larger faces, under higher biaxial tensile stresses, may contract elastically more than smaller faces while the melt cools. Biaxial tensile stresses in faces promote earlier crystallisation, with associated contraction, than in the less-orientated, thicker edges. The subsequent contraction of the edges probably caused

the faces to wrinkle. These issues were partly addressed by Almanza et al. (2004) who attempted to predict the thermal expansion coefficient of PE foams of different densities. The predicted effect of initially-bowed faces in a LDPE foam model compressed in the [1 1 1] direction, was to reduce the compressive yield stress by 11%, which is not large given the uncertainties in the polymer properties. This contrasts with the large reductions in Young's modulus and yield strength of aluminium foams predicted by Simone and Gibson (1998) using a half cell high Kelvin model compressed in the [0 0 1] direction (however aluminium has a much smaller yield strain than LDPE).

FEA predicted that LDPE foams recover more after impact than EPS foams of the same density, and that the residual strain increased with the foam impact deformation. LDPE has a higher tensile yield strain than polystyrene, and the initial compressive yield stress of LDPE foam is about one seventh of that of the same density EPS foam. The plastic hinges in LDPE foam faces are less sharp than those in EPS, while viscoelastic processes are more marked in LDPE. Hence the compressed cell air in unloaded LDPE foams is more likely to cause face unbending, reverse yielding and slow recovery, than in EPS foams.

There are few signs, in samples examined after drop impacts, of inhomogeneous deformation in LDPE or EPS foams, with a high-strain region near the specimen top. In this respect, the FEA model predictions for strain rates of 50 and 500 s^{-1} are realistic. Ouellet et al. (2006) found that EPS of densities 61 and 112 kg m^{-3} compressed uniformly at strain rates circa 1000 s^{-1}. Their observed strain rate dependence of the compressive yield stress over the range 500–1500 s^{-1} was probably caused by an isothermal to adiabatic transition in the air compression conditions.

6. Conclusions

Dynamic interactions between cell air pressures and polymer face deformation have been modelled for the first time. Dynamic FEA of the dry Kelvin model made accurate quantitative predictions of the high-strain impact compressive response of closed-cell polymer foams from the polymer mechanical properties and foam density. The model had a nearly isotropic compressive yield stress. The compressive stress increase in LDPE foams, in the engineering strain range 0.1–0.6, was due to cell air compression, with the polymer contribution being nearly constant. Face-to-face contact occurred when the foam strain exceeded a value in the range 0.6–0.8. The stress increase at higher strains was due to a combination of face-to-face contact and cell air compression. FEA predicts that LDPE foams recover more after impact than EPS foams of the same density. Even at strain rates circa 500 s^{-1}, the foams are predicted to compress nearly uniformly, with pressure differentials between cells remaining less than 100 kPa.

Acknowledgements

The suggestion of one referee, how to deal with lateral motion of massless surface elements in symmetry planes, was appreciated. The validity of the FEA models was rigorously checked at the insistence of the other referee. The computer cluster 'Blue Bear' of the University of Birmingham was used for the ABAQUS analysis.

Appendix

Editing the ABAQUS input file includes (*explanations in italics*)At the start of the file, after the jobname line, add
*PHYSICAL CONSTANTS, ABSOLUTE ZERO = −273.16, UNIVERSAL GAS CONSTANT = 8314 (*R in*N mm $K^{-1}mol^{-1}$)In the *polymer* part, for each cell *j*, define a dummy node C*j*n, lying on junction of the appropriate cell symmetry surfaces. Follow this by lines defining each fluid cavity, then the fluid
*Node, Nset = C1*n*
30001, 0.583333, 0.583333, 0.583333 (*node number and coordinates*)
*FLUID CAVITY, NAME = cell*1*, REF NODE = 30001, SURFACE = cell1insurf, BEHAVIOR = GAS, AMBIENT PRESSURE = 0.1013 (*absolute pressure in N* mm^{-2})
blank line
*FLUID BEHAVIOR, NAME = GAS
*MOLECULAR WEIGHT
0.0289 (*molecular weight of air, in kg* mol^{-1})
*CAPACITY, TYPE = TABULAR (*air specific heat at constant pressure*
10000 *needed, but not relevant for an isothermal gas*)At the start of the STEP section, define a node OPC*j*n associated with each cell
*Nset, Nset = OPC1n, instance = polymer-1
C1n, *(related to C1n)*In the output history section, add for each cell
*Node Output, nset = OPC1n
CMASS, PCAV, CVOL (*the air mass, pressure and cell volume*)

References

ABAQUS 6.7, 2007. Hibbert, Karlson and Sorenson, Inc., Pawtucket, RI.
Almanza, O., Rodríguez-Pérez, M.A., de Saja, J.A., 2001. The microstructure of polyethylene foams produced by a nitrogen solution process. Polymer 42, 7117–7126.

Almanza, O., Masso-Moreu, Y., Mills, N.J., Rodríguez-Pérez, M.A., 2004. Thermal expansion coefficient and bulk modulus of polyethylene closed-cell foams. J. Poly. Sci. B Phys. 45, 3741–3749.
Almanza, O., Rodríguez-Pérez, M.A., Chernev, B., de Saja, J.A., Zipper, P., 2005. Comparative study on the lamellar structure of polyethylene foams. Euro. Polym. J. 41, 599–609.
Ankrah, S., 2003. Ph.D. thesis, Protective materials for sporting applications, University of Birmingham.
Avalle, M., Belingardi, G., Ibba, A., 2007. Mechanical models of cellular solids: parameters identification from experimental tests. Int. J. Impact Eng. 34, 3–27.
Brakke, K.A., Sullivan, J.M., 1997. Using symmetry features of the surface evolver to study foams. In: Hege, H-C., Polthier, K. (Eds.), Visualization and Mathematics: Experiments, Simulations, and Environments. Springer.
Deshpande, V.S., Fleck, N.A., 2000. High strain rate compressive behaviour of aluminium alloy foams. Int. J. Impact Eng. 24, 277–298.
Di Landro, L., Sala, G., Olivieri, D., 2002. Deformation mechanisms and energy absorption of polystyrene foams for protective helmets. Polym. Test. 21, 217–228.
Gibson, L.J., Ashby, M.F., 1997. Cellular Solids, Second ed. Cambridge University Press, Cambridge.
Gong, L., Kyriakides, S., Triantafyllis, N., 2005. On the stability of Kelvin cell foams under compressive loads. J. Mech. Phys. Solids 53, 771–794.
Loveridge, P., Mills, N.J., 1991. The mechanism of the recovery of impacted high-density polyethylene foam. Cell. Polym. 10, 393–405.
McKown, S., 2005. The progressive collapse of novel aluminium foam structures, Ph.D. thesis, University of Liverpool.
Mills, N.J., 1994. Impact response. In: Hilyard, N.C., Cunningham, A. (Eds.), Low Density Cellular Plastics. Chapman and Hall, London, pp. 270–318.
Mills, N.J., 1996. Accident investigation of motorcycle helmets. Impact 5, 46–51.
Mills, N.J., 2005. Plastics: Microstructure and Engineering Applications, Third ed. Butterworth Heinemann, London.
Mills, N.J., 2007a. Polymer Foams Handbook – Engineering and Biomechanics Applications and Design Guide. Butterworth Heinemann, London. Chapter 11.
Mills, N.J., 2007b. High strain mechanical response of wet Kelvin open-cell foams. Int. J. Solids Struct. 44, 51–65.
Mills, N.J., Gilchrist, A., 1997. The effects of heat transfer and Poisson's ratio on the compressive response of closed-cell polymer foams. Cell. Polym. 16, 87–109.
Mills, N.J., Gilchrist, A., 2007. Properties of bonded polypropylene bead foams: data and modelling. J. Mater. Sci. 42, 3177–3189.
Mills, N.J., Zhu, H., 1999. The high strain compression of closed-cell polymer foams. J. Mech. Phys. Solids 47, 669–695.
Ouellet, S., Cronin, D., Worswick, M., 2006. Compressive response of polymeric foams under quasi-static, medium and high strain rate conditions. Poly. Test. 25, 731–743.
Rusch, K.C., 1970. Load-compression behavior of brittle foams. J. Appl. Poly. Sci. 14, 1263–1276.
Santosa, S., Wierzbicki, T., 1998. On the modelling of crush behavior of a closed-cell aluminium foam structure. J. Mech. Phys. Solids 46, 645–669.
Simone, A.E., Gibson, L.J., 1998. The effects of cell face curvature and corrugations on the stiffness and strength of metal foams. Acta Mater. 46, 3929–3935.
Song, B., Chen, W.W., Dou, S., Winfree, N.A., Kang, J.H., 2005. Strain-rate effects on elastic and early cell-collapse responses of a polystyrene foam. Int. J. Impact Eng. 31, 509–521.
Stampanoni, M., Groso, A., Isenegger, A. Mikuljan., G., Chen, Q., Bertrand, A., Henein, S., Betemps, R., Frommherz, U., Bühler, P., Meister, D. Lange, M., Abela, R., 2006. Trends in synchrotron-based tomographic imaging: the SLS experience. In: Proceedings of the SPIE, Devel, in X-ray Tomography, 6318 pp.
Stauffer, F., 2007. Sandwich-Strukturen für ein besseres Dämpfungsverhalten in Polystyrol-basierten Helmen, M.Sc. thesis, ETH, Zürich.
Willinger, R., Baumgartner, D., Guimberteau, T., 2000. Dynamic characterization of motorcycle helmets: modelling and coupling with the human head. J. Sound Vibr. 235, 611–625.
Zheng, Z., Yu, J., Li, J., 2005. Dynamic crushing of 2D cellular structures: a finite element study. Int. J. Impact Eng. 32, 650–664.
Zhu, H., Mills, N.J., Knott, J.F., 1997. Analysis of the high strain compression of open-cell foams. J. Mech. Phys. Solids 45, 1875–1904.